Experimental demonstration of the mechanism of steady-state microbunching

Xiujie Deng[1], Alexander Chao[2,3], Jörg Feikes[4,*], Arne Hoehl[5], Wenhui Huang[1], Roman Klein[5], Arnold Kruschinski[4], Ji Li[4], Aleksandr Matveenko[4], Yuriy Petenev[4], Markus Ries[4], Chuanxiang Tang[1,*] & Lixin Yan[1]

[1]*Department of Engineering Physics, Tsinghua University, Beijing 100084, China.*

[2]*Institute for Advanced Study, Tsinghua University, Beijing 100084, China.*

[3]*Stanford University, Stanford, California 94309, USA.*

[4]*Helmholtz-Zentrum Berlin (HZB), Albert-Einstein-Straße 15, 12489 Berlin, Germany.*

[5]*Physikalisch-Technische Bundesanstalt (PTB), Abbestraße 2-12, 10587 Berlin, Germany.*

Particle accelerators as photon sources have been fostering advances in science and technology[1]. Currently the workhorses of these sources are storage ring-based synchrotron radiation facilities (SRs)[2-4] and linac-based free-electron lasers (FELs)[5-14]. SRs deliver photons with high repetition rate but relatively low power due to their temporally incoherent nature. FELs produce radiation with high peak brightness while the repetition rate is limited by the driving sources. A mechanism called steady-state microbunching[15-22] (SSMB) has been proposed to generate high-repetition high-brightness radiation, at wavelengths ranging from the terahertz to extreme ultraviolet. It accomplishes this by utilizing the microbunching-enabled multiparticle coherent enhancement of radiation in an

electron storage ring on a steady-state turn-by-turn basis. Here we report the first experimental demonstration of the mechanism of SSMB. We have shown that electron bunches stored in a quasi-isochronous ring can yield sub-μm microbunching and coherent radiation, one complete revolution after a 1064-nm-wavelength laser-induced energy modulation. The results verify that the optical phases of electrons can be correlated turn-by-turn in a sub-laser-wavelength precision. Based on this turn-by-turn phase correlation, SSMB can be anticipated by applying a phase-locked laser to interact with the electrons turn-by-turn. This demonstration represents the first milestone in the development of SSMB photon sources.

Coherent radiation is a powerful radiation scheme, as the intensity is proportional to the number of emitters – squared, in contrast to incoherent radiation that is proportional to the number of emitters. To obtain coherent radiation from an electron beam, the particles need to be bunched or sub-bunched to longitudinal dimensions smaller than the radiation wavelength[23-25]. For a short wavelength of interest, such a bunch or sub-bunches are referred to as microbunching. The great potential of microbunching has been exemplified by the free-electron lasers[5-14], which produce short pulses of radiation with high peak brightness. However, linac-driven FELs use each electron bunch once, limiting the repetition rate and average power of the radiation. A mechanism called steady-state microbunching (SSMB) has been proposed in ref. 15 to tackle this challenge. The idea of SSMB is to manipulate the particle dynamics in a storage ring, so that the electron bunch length is not in the usual cm-to-mm range, but in the range ~ μm or shorter. By exploiting the microbunching in a turn-by-turn steady state, SSMB envisages radiation with high power, high repetition rate (MHz to continuous-wave) and narrow linewidth, at wavelengths ranging from the terahertz to extreme ultraviolet (EUV).

Such a novel photon source promises unprecedented opportunities for accelerator photon science and technological applications. For example, SSMB is one of the promising schemes to generate the high-power EUV radiation for EUV lithography[26]. The energy-tunable high-flux narrowband EUV photons are also highly desirable in condensed matter physics study, like angle-resolved photoemission spectroscopy[27,28]. Ultrahigh-power deep ultraviolet and infrared sources are potential research tools in atomic and molecular physics. Moreover, new nonlinear phenomena and dynamical properties of materials can be driven and studied by high peak and average power terahertz sources[29,30]. Besides the high power, SSMB can also produce ultrashort (sub-femtosecond to attosecond) photon pulse and pulse trains with definite phase relations, which could be useful in attosecond physics investigations[31].

To realize SSMB, laser modulators are invoked as the bunching systems. A typical laser modulator comprises a laser and an undulator, in which the undulator makes the electrons undergo transverse oscillations and the co-propagating laser exchanges energy with the electrons. Ignoring radiation energy loss, the longitudinal dynamics of a particle in a storage ring with a laser modulator is described by the one-turn map

$$\delta_{n+1} = \delta_n + A\sin(k_{\mathrm{L}} z_n + \phi_{\mathrm{s}}),\ z_{n+1} = z_n - C_0\eta\delta_{n+1}, \quad (1)$$

where $\delta = \Delta E/E_0$ and z are the relative energy deviation and longitudinal displacement of the particle, with E_0 being the energy of the reference (synchronous) particle, A is the E_0-normalized energy modulation amplitude induced by the laser, $k_\mathrm{L} = 2\pi/\lambda_\mathrm{L}$ is the laser wavenumber, ϕ_s are the synchronous phases spaced by 2π, C_0 is the ring circumference, $\eta = \frac{\Delta T}{T_0}/\frac{\Delta E}{E_0}$ is the phase slippage factor of the ring and is a measure for the energy dependence of revolution period for the particle, in which T_0 is the revolution period of the reference particle. With this one-turn map established, the laser modulator supplies the longitudinal focusing and phase stabilization of the particles, similarly to the functions provided by the conventional radiofrequency (RF) cavity via the phase stability principle[32,33]. As a result, the particles are microbunched around the synchronous phases with a spacing of the laser wavelength.

There are continuous development on other electron manipulation techniques in accelerators, using actively applied laser fields[34-37] or electron-self-generated fields[38,39], to tailor the radiation properties. Dedicated efforts have also been devoted to storage ring FELs, like the European UV/VUV FEL at ELETTRA[40,41]. The unique characteristic of SSMB lies in the precise turn-by-turn phase space correlation which eliminates the accumulative electron beam energy heating and emittance (average spread of particle coordinates in the phase space) growth.

At the Metrology Light Source[42,43] (MLS) of the Physikalisch-Technische Bundesanstalt in Berlin, we have demonstrated experimentally that sub-μm microbunching is achievable after one complete revolution of a 1064-nm-wavelength laser-modulated electron bunch in a quasi-isochronous ring. This demonstration proves that the longitudinal dynamics described by the one-turn map Eq. (1) can be extrapolated from the RF wavelength (~ m) to laser wavelength (~ μm) for a stored electron beam, therefore validates the SSMB microbunching mechanism.

The schematic of the experiment setup is illustrated in Fig. 1. A horizontally polarized laser pulse (wavelength $\lambda_{\mathrm{L}} = 1064\ \mathrm{nm}$, full-width at half-maximum, FWHM ~ 10 ns, energy ~ 50 mJ) is sent into a planar undulator (period $\lambda_{\mathrm{U}} = 0.125$ m, total length 4 m), to co-propagate with the electron bunches (energy $E_0 = 250$ MeV) stored in the MLS storage ring (circumference $C_0 = 48$ m). To maximize the laser-electron energy exchange, the undulator gap is chosen to let the resonant condition $\lambda_{\mathrm{S}} = \lambda_{\mathrm{L}}$ be satisfied, where $\lambda_{\mathrm{S}} = \frac{(1+K^2/2)}{2\gamma^2}\lambda_{\mathrm{U}}$ is the central wavelength of the spontaneous undulator radiation, with $\gamma \propto E_0$ being the Lorentz factor and $K = 2.5$ being the deflection parameter determined by the undulator period and magnetic field strength. This laser-electron interaction induces a sinusoidal energy modulation pattern with a period of the laser wavelength on the electron beam. As particles with different energies have different revolution periods, after one revolution in the ring, the energy-modulated electrons shift longitudinally with respect to each other, clumping towards the synchronous phases and forming microbunches. The above experiment processes are modeled by Eq. (1) and the coherent undulator radiation generated from the microbunches is then detected, by a high-speed photodetector with photodiode, as the evidence of microbunching.

The low beam energy $E_0 = 250\ \mathrm{MeV}$ is employed to mitigate the stochastic quantum radiation excitation[44,45,22], which brings the diffusion of the longitudinal coordinate z and can wash out fine longitudinal bunch structures at higher beam energy (see Methods). A lower beam energy at the same time gives a smaller equilibrium relative energy spread σ_δ (root-mean-square, r.m.s.), as $\sigma_\delta \propto \gamma$. The spread of z during recirculation, from the uncorrelated energy spread, then becomes smaller and is favourable for microbunching. At $E_0 = 250\ \mathrm{MeV}$, we have $\sigma_\delta = 1.8 \times 10^{-4}$. Since the laser wavelength is much smaller than that of an RF cavity, the phase slippage factor η needs to be ultra-small, i.e., the ring should be quasi-isochronous[46], to allow the turn-by-turn stabilization of the electron optical phases for particles with different energies. In the experiment, the MLS has been pushed close to the isochronous point with $\eta \approx -2 \times 10^{-5}$ (see Methods), which is three orders of magnitude smaller than its standard value 3×10^{-2}. By implementing these parameters, the r.m.s. spread of z in one turn arising from the uncorrelated energy spread is $\Delta z_{\mathrm{ES}} = |C_0 \eta \sigma_\delta| \approx 0.17\ \mu\mathrm{m}$ (~ 0.6 fs), making the formation and sustain of sub-μm microbunching possible.

The long-pulse laser (FWHM ~ 10 ns) is applied to simplify the experiment by avoiding a dedicated laser-electron synchronization system, since the shot-to-shot laser timing jitter $t_{\mathrm{jitter}} \leq 1\ \mathrm{ns}$ (r.m.s.). However, the photodetector (Femto HSPR-X-I-1G4-SI, rise/fall time 250 ps) is saturated and even damaged by the powerful laser (Beamtech Optronics Dawa-200) if it is placed in the path of the laser. To alleviate this issue, the undulator radiation is separated into the fundamental and second harmonics, by appropriate dichroic mirrors (Thorlabs Harmonic Beamsplitters HBSY21/22), and the signal detection focuses on the second harmonic with the wavelength centered at 532 nm as shown in Fig. 1. The photodetector output voltage, which is proportional to the radiation power, is then measured by a digital oscilloscope (Tektronix MSO64:6-BW-4000, 4 GHz bandwidth, 25 GS/s sample rate).

Figure 2 shows the typical measurement results of the second-harmonic undulator radiation emitted from a homogeneous stored bunch train, with a charge of ~ 1 pC/bunch (see Methods) and a time spacing of 2 ns given by the 500 MHz RF cavity at the MLS. The spikes in the waveforms are the signals of different bunches. The left and right panels are the results corresponding to 2 and 40 consecutive laser shots, respectively. To smooth the measurement noise and signal fluctuation, the waveforms in the right panel have been averaged. Figure 2a and b illustrate the signals one turn before the laser shot, so they are the usual incoherent radiation and reflect the homogenous bunch filling pattern. Figure 2c and d show the radiation one turn after the laser shot, from the same bunches in obtaining Fig. 2a and b. The five larger spikes in the center correspond to the bunches modulated by the laser. The enhanced signals of these five spikes indicate the formation of microbunching and generation of coherent radiation from the laser-modulated bunches.

The Q-switched laser used in the experiment has multiple longitudinal modes, and its temporal profile has several peaks and fluctuates significantly from shot to shot (see Extended Data Fig. 2). Therefore, the laser-induced electron energy modulation amplitudes are different from shot to shot, and also from bunch to bunch. When the modulation amplitude matches the phase slippage factor, the energy-modulated electrons are properly focused at the synchronous phases and this gives optimal microbunching (see Methods). For some of the shots, the laser intensity is higher or lower than the optimal value, and the electrons are then over-focused or under-focused, giving weaker microbunching and less coherent radiation. This explains the shot-to-shot fluctuation of the coherent amplified signals shown in Fig. 2c and e.

Due to the definite phase relation imprinted by the laser, the spectrum of the coherent radiation from microbunching is Fourier transform-limited. Then, there is $\left(\frac{\Delta\lambda}{\lambda}\right)_{\mathrm{FWHM}} < 0.4\%$ for the second-harmonic coherent radiation. This is because the electron bunch length in the experiment is expected to be larger than the theoretical zero-current value[44] of 0.12 ps (r.m.s.), considering bunch lengthening effects such as the RF phase noise. In contrast, the bandwidth of the incoherent radiation is $\frac{1}{2N_{\mathrm{U}}} \approx 1.6\%$ (FWHM) on axis and even broader taking into account the off-axis redshifted part (~ 10% within the aperture at detection based on SPECTRA[47] calculation), with $N_{\mathrm{U}} = 32$ being the number of undulator periods. To confirm that the amplified radiation is owing to microbunching, this narrowband feature of the coherent radiation is tested. A 532-nm-center-wavelength 3-nm-bandwidth (FWHM) band-pass filter (Thorlabs FL532-3) is inserted in front of the detector. The radiation one turn after the laser shot is shown in Fig. 2e and f, which is obtained with a similar bunch filling and charge as that of Fig. 2c and d. From the comparison between Fig. 2e and 2c (2f and 2d), we can see that the broadband incoherent signals are nearly completely blocked by the filter while the amplified part is not much affected, confirming that the amplification is the narrowband coherent radiation generated from the microbunches.

Finally, the bunch-charge dependence of the coherent radiation is investigated. To mitigate collective effects like intrabeam scattering[48,49] and head-tail instability[50] which could change the electron beam parameters, this investigation is conducted at low beam current and the coherent signal is optimized by fine-adjusting the machine (see Methods) to assure a sufficient signal-to-noise ratio. As the longitudinal radiation damping time[44] in the experiment is 180 ms, we operate the laser at 1.25 Hz repetition rate to ensure that the electron bunches have time to recover their equilibrium parameters before each laser shot. The 3-nm-bandwidth band-pass filter is inserted to block the incoherent radiation, and the coherent signal corresponding to each individual laser shot have been saved, with the beam current decaying naturally until the signal is at the detection noise level. The measurement results of the bunch closest to the laser temporal center ($t = 0\ \mathrm{ns}$ in Fig. 2) are used for quantitative analysis (see Methods). To smooth the impact of the laser temporal profile fluctuation and measurement noise, a 200-consecutive-laser-shots averaging is performed in obtaining the data point for each bunch charge. The coherent undulator radiation power versus single-bunch charge is shown in Fig. 3, in which a quadratic function fits well with the experiment data. The quadratic bunch-charge dependence, together with the narrowband feature of the coherent radiation, demonstrates unequivocally the microbunching formation.

We point out that this paper is not reporting the actual demonstration of SSMB, but rather the demonstration of the mechanism by which SSMB will eventually be attained. Firstly, the microbunching formation, after one complete revolution of a laser-modulated bunch in a quasi-isochronous ring, demonstrates the viability of a turn-by-turn electron optical phase correlation with a precision of sub-laser-wavelength. Secondly, this microbunching is produced on the stored electron bunch whose equilibrium parameters and distribution before the laser modulation are defined by the same storage ring as a whole. The combination of these two crucial ingredients establishes a closed loop to support the realization of SSMB, provided there is a phase-locked laser to interact with the electrons turn-by-turn.

In conclusion, the mechanism of SSMB has been demonstrated the first time in an electron storage ring. On the basis of the achieved result, the next stage to sustain the microbunching for multiple turns, by replacing the present laser with a high-repetition phase-locked one, is ongoing at the MLS.

1. Chao, A. W. & Chou, W. *Reviews of Accelerator Science and Technology - Volume 3: Accelerators as Photon Sources* (World Scientific, 2011).
2. Elder, F. R., Gurewitsch, A. M., Langmuir, R. V. & Pollock, H. C. Radiation from electrons in a synchrotron. *Phys. Rev.* **71**, 829 (1947).
3. Schwinger, J. On the classical radiation of accelerated electrons. *Phys. Rev.* **75**, 1912 (1949).
4. Zhao, Z. T. Storage ring light sources. *Reviews of Accelerator Science and Technology* **3**(01), 57-76 (2010).

5. Madey, J. M. Stimulated Emission of Bremsstrahlung in a Periodic Magnetic Field. *J. Appl. Phys.* **42**, 1906 (1971).
6. Deacon, D. A. G. et al. First Operation of a Free-Electron Laser. *Phys. Rev. Lett.* **38**, 892 (1977).
7. Billardon, M. et al. First Operation of a Storage-Ring Free-Electron Laser. *Phys. Rev. Lett.* **51**, 1652 (1983).
8. Kondratenko, A. & Saldin, E. Generating of coherent radiation by a relativistic electron beam in an ondulator. *Part. Accel.* **10**, 207-216 (1980).
9. Bonifacio, R., Pellegrini, C. & Narducci, L. Collective instabilities and high-gain regime in a free-electron laser. *Opt. Commun.* **50**, 373-378 (1984).
10. Hogan, M. et al. Measurements of gain larger than 10^5 at 12 μm in a self-amplified spontaneous-emission free-electron laser. *Phys. Rev. Lett.* **81**, 4867–4870 (1998).
11. Andruszkow, J. et al. First observation of self-amplified spontaneous emission in a free-electron laser at 109 nm wavelength. *Phys. Rev. Lett.* **85**, 3825–3829 (2000).
12. Milton, S. et al. Exponential gain and saturation of a self-amplified spontaneous emission free-electron laser. *Science* **292**, 2037–2041 (2001).
13. Emma, P. et al. First lasing and operation of an ångstrom-wavelength free-electron laser. *Nat. Photonics* **4**, 641 (2010).
14. Seddon, E. A., et al. Short-wavelength free-electron laser sources and science: a review. *Rep. Prog. Phys.* **80**, 115901 (2017).
15. Ratner, D. F. & Chao, A. W. Steady-State Microbunching in a Storage Ring for Generating Coherent Radiation. *Phys. Rev. Lett.* **105**, 154801 (2010).

16. Ratner, D. & Chao, A. Reversible Seeding in Storage Rings. *In Proc. of the 33th International Free-electron Laser Conference* (JACoW, 2011); https://accelconf.web.cern.ch/AccelConf/FEL2011/papers/mopb23.pdf.

17. Jiao, Y., Ratner, D. F., & Chao, A. W. Terahertz coherent radiation from steady-state microbunching in storage rings with X-band radio-frequency system. *Phys. Rev. ST Accel. Beams* **14**, 110702 (2011).

18. Chao, A. et al. High Power Radiation Sources using the Steady-state Microbunching Mechanism. In *Proc. of the 7th International Particle Accelerator Conference* (JACoW, 2016); http://accelconf.web.cern.ch/AccelConf/IPAC2016/papers/tuxb01.pdf.

19. Tang, C. et al. An Overview of the Progress on SSMB. In *Proc. of the 60th ICFA Advanced Beam Dynamics Workshop on Future Light Sources* (JACoW, 2018); http://accelconf.web.cern.ch/AccelConf/fls2018/papers/thp2wb02.pdf.

20. Chao, A. et al. A Compact High-Power Radiation Source Based on Steady-State Microbunching Mechanism. Tech. Rep. SLAC-PUB-17241 (2018).

21. Deng, X. et al. From Coherent Harmonic Generation to Steady State Microbunching. In *Proc. of the 9th International Particle Accelerator Conference* (JACoW, 2018); https://accelconf.web.cern.ch/AccelConf/ipac2018/papers/thpmk113.pdf.

22. Deng, X. J., Chao, A. W., Feikes, J., Huang, W. H., Ries, M., & Tang, C. X. Single-particle dynamics of microbunching. *Phys. Rev. Accel. Beams* **23**, 044002 (2020).

23. Nodvick, J. S., & David S. S. Suppression of coherent radiation by electrons in a synchrotron. *Phys. Rev.* **96**, 180 (1954).

24. Williams, G. P. et al. Coherence effects in long-wavelength infrared synchrotron radiation emission. *Phys. Rev. Lett.* **62**, 261 (1989).

25. Gover, A. et al. Superradiant and stimulated-superradiant emission of bunched electron beams. *Rev. Mod. Phys.* **91,** 035003 (2019).

26. Bakshi, V. *EUV Lithography*, 2nd ed. Vol. **149** (SPIE Press, 2018).

27. Damascelli, A., Hussain, Z., & Shen, Z. X. Angle-resolved photoemission studies of the cuprate superconductors. *Rev. Mod. Phys.* **75**, 473 (2003).

28. Lv, B., Qian, T. & Ding, H. Angle-resolved photoemission spectroscopy and its application to topological materials. *Nat Rev Phys* **1**, 609–626 (2019).

29. Carr, G., Martin, M., McKinney, W. et al. High-power terahertz radiation from relativistic electrons. *Nature* **420**, 153–156 (2002).

30. Cole, B. E.,Williams, J. B. & King, B. T. Coherent manipulation of semiconductor quantum bits with terahertz radiation. *Nature* **410**, 60–63 (2001).

31. Krausz, F. & Misha I. Attosecond physics. *Rev. Mod. Phys.* **81**, 163 (2009).

32. Veksler, V. I. New method for the acceleration of relativistic particles. *Doklady Akademii Nauk USSR* **43**, 346-348 (1944).

33. McMillan, E. M. The Synchrotron—A Proposed High Energy Particle Accelerator. *Phys. Rev.* **68**, 143 (1945).

34. Girard, B. et al. Optical Frequency Multiplication by an Optical Klystron. *Phys. Rev. Lett.* **53**, 2405 (1984).

35. Yu, L. H. Generation of intense uv radiation by subharmonically seeded single-pass free-electron lasers. *Phys. Rev. A* **44**, 5178 (1991).

36. Yu, L.-H. et al. High-Gain Harmonic-Generation Free-Electron Laser. *Science* **289**, 932-934 (2000).

37. Hemsing, E., Stupakov, G., Xiang, D., & Zholents, A. Beam by design: Laser manipulation of electrons in modern accelerators. *Rev. Mod. Phys.* **86**, 897 (2014).

38. Byrd, J. M. et al. Observation of broadband self-amplified spontaneous coherent terahertz synchrotron radiation in a storage ring. *Phys. Rev. Lett.* **89**, 224801 (2002).

39. Venturini, M. & Robert W. Bursts of coherent synchrotron radiation in electron storage rings: a dynamical model. *Phys. Rev. Lett.* **89**, 224802 (2002).

40. Walker, R. P. et al. First lasing and initial performance of the European UV/VUV storage ring FEL at ELETTRA. *Nucl. Instr. and Meth. A* **475**, 20 (2001).

41. Trovo, M. et al. Operation of the European storage ring FEL at ELETTRA down to 190 nm. *Nucl. Instr. and Meth. A* **483**, 157 (2002).

42. Feikes, J. et al. Metrology Light Source: The first electron storage ring optimized for generating coherent THz radiation. *Phys. Rev. ST Accel. Beams* **14**, 030705 (2011).

43. Ries, M. Nonlinear Momentum Compaction and Coherent Synchrotron Radiation at the Metrology Light Source. Dissertation, Humboldt University of Berlin, Berlin, Germany (2014).

44. Sands, M. The physics of electron storage rings: an introduction. Tech. Rep. SLAC-121 (1970).

45. Shoji, Y., Tanaka, H., Takao, M. & Soutome, K. Longitudinal radiation excitation in an electron storage ring. *Phys. Rev. E* **54**, R4556 (1996).

46. Pellegrini, C. & Robin, D. Quasi-isochronous storage ring. *Nucl. Instrum. Methods Phys. Res., Sect. A* **301**, 27-36 (1991).

47. Tanaka, T. & Hideo K. SPECTRA: a synchrotron radiation calculation code. *J. Synchrotron Rad.* **8**, 1221-1228 (2001).

48. Piwinski, A. Intra-beam scattering. Tech. Rep. No. DESY-H1-73-3. 1974.

49. Bjorken, J. D. & Mtingwa, S. K. Intrabeam scattering. *Part. Accel.* **13**. FERMILAB-PUB-82-47-THY (1982): 115-143.

50. Chao, A. W. *Physics of collective beam instabilities in high energy accelerators*. (Wiley, 1993).

Methods

Electron beam energy. When a relativistic electron is subjected to acceleration normal to its velocity exerted by a bending magnet, it radiates electromagnetic energy[2,3]. This radiation is characterized by the quantum nature of the photon emission process. The photon energy and place of emission are both stochastic, giving rise to changes on particle energy[44] (instantly) and the longitudinal coordinate[45,22] z (non-instantly). Of special interest in the experiment is the r.m.s. quantum diffusion of z in one turn[45,22]

$$\Delta z_{\mathrm{QE}} = C_0 \sqrt{I_{\tilde{\eta}} \langle N \rangle \langle \frac{u^2}{E_0^2} \rangle} \quad (2)$$

where $I_{\tilde{\eta}}$ is the variance of partial phase slippage factors defined as the phase slippages from the emission positions to an observation point, N is the number of photons emitted in one turn, u is the photon energy, and the brackets represent statistical expectation. For the MLS quasi-isochronous magnet lattice (see Extended Data Fig. 1), Δz_{QE} is as large as 260 nm at its standard operation energy of 630 MeV, deteriorating the sub-μm microbunching considerably. Therefore, the beam energy needs to be lowered to mitigate this diffusion, as $\sqrt{\langle N \rangle \langle \frac{u^2}{E_0^2} \rangle} \propto \gamma^{2.5}$. A lower beam energy at the same time gives a smaller energy spread and is also beneficial for microbunching as explained in the main text. Nevertheless, the beam energy cannot be too low, otherwise the beam parameters and lifetime can be profoundly affected by the scattering among particles[48,49,51]. An electron beam energy of 250 MeV is adopted in the experiment to balance these issues.

Quasi-isochronous storage ring. To form and sustain microbunching in a storage ring, the r.m.s. spread of z in one turn arising from the uncorrelated electron energy spread should be adequately smaller than the laser wavelength, i.e.,

$$\Delta z_{\mathrm{ES}} = |C_0 \eta \sigma_\delta| \lesssim \lambda_{\mathrm{L}}/2\pi \quad (3)$$

To fulfill this requirement, the phase slippage factor of the MLS has been lowered to $\eta \approx -2 \times 10^{-5}$. Such a quasi-isochronous magnet lattice is achieved by tailoring the horizontal dispersion functions D_x (a measure for the energy dependence of horizontal position for the particle) around the ring, so that a particle with non-ideal energy travels part of the ring inwards and part of the ring outwards compared to the reference orbit, thus having a revolution period nearly the same as that of the ideal particle. The tailoring of D_x is accomplished by adjusting the quadrupole magnet (de)focusing strengths. The operation of the MLS as a quasi-isochronous ring also benefits from the optimization of the sextupole and octupole nonlinear magnet schemes to control the higher-order terms of the phase slippage[42,43], which affect both the equilibrium beam distribution before the laser modulation and the succeeding microbunching evolution[22].

In the experiment, the value of the small phase slippage factor is quantified by measuring the electron orbit offsets, when we slightly adjust the RF frequency up and down, at a beam position monitor (BPM) where D_x is large. From the offsets and D_x, the phase-slippage-dependent electron energy shifts caused by the RF frequency adjustment can be derived, thus also the phase slippage factor. The D_x at the BPM is acquired using the same method in the opposite way, i.e, based on a known phase slippage factor. This is done at a larger phase slippage factor where its value can be determined from its relation with the longitudinal oscillation, usually referred to as synchrotron oscillation in accelerator physics, frequency of the electron beam[44]. The synchrotron oscillation frequency can be measured accurately at a phase slippage factor like -5×10^{-4} and it has been confirmed in the model that the relative change of D_x at the highly dispersive BPM is small (< 4%) when the phase slippage factor is reduced from -5×10^{-4} to the desired -2×10^{-5}, by changing the quadrupole magnet strengths marginally.

Matching of laser intensity with storage ring phase slippage. With the electron beam evolved according to Eq. (1) for one revolution in the ring, the degree of microbunching at the n^{th} laser harmonic can be quantified by the parameter bunching factor[35]

$$b_n = \left|\langle e^{ink_{\mathrm{L}}z}\rangle\right| = \left|J_n(nk_{\mathrm{L}}C_0\eta A)\exp\left[-\frac{(nk_{\mathrm{L}}C_0\eta\sigma_\delta)^2}{2}\right]\right| \quad (4)$$

where J_n is the Bessel function of the first kind. The coherent radiation power at the n^{th} harmonic is proportional to the bunching factor squared $|b_n|^2$. For a given phase slippage factor and harmonic number, there is an optimal laser-induced energy modulation amplitude A ($A\propto\sqrt{P}$ and P is the laser power) that gives the maximum bunching factor. Putting $\eta=-2\times10^{-5}$ and other related parameters in Eq. (4), $A\approx 1.5\sigma_\delta$ results the largest second-harmonic bunching.

Transverse-longitudinal coupling. Apart from the longitudinal beam dynamics, the coupling of the particle transverse motion, usually called betatron oscillation in accelerator physics, to the longitudinal dimension is also critical. The reason is based on the fact that the horizontal beam width at the undulator is ~ 600 μm (model), three orders of magnitude larger than the sub-μm longitudinal structures we aim to produce. As the vertical emittance is much smaller than the horizontal one in a planar storage ring, in the following only the impact of the horizontal betatron oscillation is considered.

The r.m.s. bunch lengthening of an electron beam longitudinal slice after n complete revolutions in the ring, due to betatron oscillation, is[51,53,22]

$$\Delta z_{\mathrm{B,n}} = 2\sqrt{\epsilon_x H_x}|\sin(n\pi\nu_x)| \quad (5)$$

where $\epsilon_x = \langle J_x \rangle$ is the beam emittance, with the brackets denoting particle ensemble average and $J_x = \left(\gamma_x x^2 + 2\alpha_x x x' + \beta_x x'^2\right)/2$ being the particle betatron action, x and x' being the horizontal position and angle of the particle, $\alpha_x, \beta_x, \gamma_x$ being the Courant-Snyder functions[54] of the storage ring, $H_x = \gamma_x {D_x}^2 + 2\alpha_x D_x D_x' + \beta_x {D_x'}^2$ (D_x' is the dispersion angle) is the chromatic function[44] which quantifies the degree of transverse-longitudinal coupling and ν_x is the number of betatron oscillations per revolution. Putting in $\epsilon_x = 31$ nm (model) and $\nu_x = 3.18$ (model and measured), we need $H_x \leq 0.8$ μm at the undulator to have $\Delta z_{\mathrm{B,1}} \leq \lambda_{\mathrm{L}}/2\pi$. This stringent condition (H_x at other places of the ring is typically $\gtrsim 0.1$ m) is satisfied by fine-adjusting the quadrupole magnet (de)focusing strengths to correct the dispersion D_x and dispersion angle D_x' at the undulator to the level of mm and 0.1 mrad, respectively (see Extended Data Fig. 1).

In addition to the linear-order oscillating bunch lengthening, the betatron oscillation also produces an average path lengthening or shortening (second-order effect) summarized by the formula[55-57]

$$\Delta C_B = -2\pi J_x \xi_x \quad (6)$$

with ΔC_B being the average change of the particle recirculation path length, and $\xi_x = d\nu_x/d\delta$ being the horizontal chromaticity of the ring. As different particles have different betatron oscillation amplitudes (actions), this effect results in a loss of synchronization between particles and degrades microbunching. Moreover, it will broaden the equilibrium energy spread and distort the beam from Gaussian[57] before the laser modulation, which also impacts the microbunching. Therefore, the horizontal chromaticity should be small to moderate its detrimental outcome, while simultaneously sufficient to suppress collective effects like the head-tail instability[50]. As a consequence, $\xi_x = -0.5$ is applied in the experiment.

Bunch charge measurement and evaluation. The bunch-by-bunch charge (current) in the experiment is measured by a single-bunch current monitor[58] which analyzes the electron beam-induced RF signals from a set of 4 stripline electrodes (3 GHz bandwidth). To minimize the influences from neighbouring bunches on the signal, the pulse response of the electrodes has been reshaped by a 500 MHz low-pass filter. The current calibration of the monitor has been conducted using a parametric current transformer[59] at higher current, and the linearity of the system at lower current is checked with the signal of the photodiode illuminated by synchrotron radiation. During the current decaying in the experiment, one data point of the result given by the monitor is saved every second for each individual bunch. The averaged measurement of 10 unfilled bunches preceding the homogenous filled bunches (10 ns time gap in between) is used as the systematic offset. To smooth the measurement noise and at the same time account for the change of beam lifetime, the time evolution of the offset-removed data points is then fitted by the sum of two exponential functions $Q(t) = Q_1 \exp(-t/\tau_1) + Q_2 \exp(-t/\tau_2)$ at different time intervals, with the fit results connected smoothly. One example evaluation of the bunch charge measurement result is presented in Extended Data Fig. 3. Based on the evaluated data, a linear bunch-charge dependence of the broadband incoherent signal, detected by the photodetector without the 3-nm-bandwidth band-pass filter, is obtained as expected and shown in Extended Data Fig. 4, confirming the reliability of the bunch charge measurement and evaluation method.

Radiation signal evaluation. To avoid the impact of the signal waveform offset caused by the laser stray light (see Fig. 2), the data analysis takes the peak-peak value of the photodetector output voltage as a measure for the radiation power. The coherent radiation power corresponding to each individual laser shot, obtained during a time interval with a decaying beam current, is presented in Extended Data Fig. 5a in which the modest contribution on the measured quantity from the slight incoherent radiation transmitted through the 3-nm-bandwidth band-pass filter has been eliminated. As can be seen, the coherent signal fluctuates significantly from shot to shot. This is attributable to the shot-to-shot fluctuation of the laser intensity profile (see Extended Data Fig. 2) and the measurement noise. In spite of the fluctuation, quadratic functions fit reasonably with the lower and upper bounds of the data points, which correspond to the cases of minimum and maximum bunching factors induced by the fluctuating laser, respectively. When performing the fits, we have taken into account that the measured quantity is the real radiation signal convoluted with the detection noise. The impact of this noise, obtained by analyzing the measurement result of the unfilled bunches, on the bounds of the measured data points is visualized in Extended Data Fig. 5a as shades for the coherent signal, and similarly in Extended Data Fig. 4a for the incoherent signal. To smooth this shot-to-shot fluctuation, a 200-consecutive-laser-shots averaging is conducted and the results are presented in Extended Data Fig. 5b and 4b for the narrowband coherent and broadband incoherent signals, in which a quadratic and a linear fit have been performed, respectively.

51. Bernardini, C. et al. Lifetime and beam size in a storage ring. *Phys. Rev. Lett.* **10**, 407 (1963).
52. Shoji, Y. Bunch lengthening by a betatron motion in quasi-isochronous storage rings. *Phys. Rev. ST Accel. Beams* **7**, 090703 (2004).
53. Shimada, M. et al. Transverse-Longitudinal Coupling Effect in Laser Bunch Slicing. *Phys. Rev. Lett.* **103**, 144802 (2009).
54. Courant, E, D & Snyder, H. S. Theory of the alternating-gradient synchrotron. *Ann. Phys.* **3**(1), 1-48 (1958).
55. Shoji, Y. Dependence of average path length betatron motion in a storage ring. *Phys. Rev. ST Accel. Beams* **8**, 094001 (2005).
56. Machida, S. et al. Amplitude-dependent orbital period in alternating gradient accelerators. *Prog. Theor. Exp. Phys.* **2016**, 033G01 (2016).
57. Deng, X. J. et al. Widening and distortion of the particle energy distribution by chromaticity in quasi-isochronous rings. *Phys. Rev. Accel. Beams* **23**, 044001 (2020).

58. Falkenstern, F., Hoffmann, F., Kuske, P., & Kuszynski, J. Bunch View-A Fast and Accurate Bunch-by-Bunch Current Monitor. *Proceedings of DIPAC09*, Basel, Switzerland. P1-3 (2009).

59. Klein, R., et al. Operation of the Metrology Light Source as a primary radiation source standard. *Phys. Rev. ST Accel. Beams* **11**, 110701 (2008).

Data and code availability The raw data from this experiment and the computer codes used for the data analysis can be downloaded at https://datadryad.org/stash/share/2PxVYaAh7bctHln3P8Ha5Q-jcnuDEGxNgYSlA4eJBYE. (doi:10.5061/dryad.r7sqv9s9f)

Acknowledgements This work is partially supported by the Tsinghua University Initiative Scientific Research Program No. 20191081195, China. We also appreciate the continuous support of A. Jankowiak (HZB) and M. Richter (PTB) which makes the experiment possible.

Author Contributions A.C. is one of the authors who conceived the original SSMB theoretical concept and has been promoting the SSMB research and collaboration. Together with A.C., the Tsinghua SSMB group, led by C.T., initiated the experiment. J.F., J.L. and M.R. prepared the setup of the storage ring for the experiment and together with Y.P. and A.M. performed the experiment at the MLS. L.Y., W.H., C.T. and X.D. designed and developed the laser scheme and related optical system. R.K., A.H. and L.Y. set up the laser system and the laser beam control as well as the coherent detection part and together with A.K. performed the experiment. X.D. defined the experimental parameters set, conducted the simulations, analyzed the beam dynamics and experimental data. X.D. wrote the paper, with revisions from A.C., J.F., M.R. and C.T. All authors participated the experiment.

Competing Interests The authors declare that they have no competing financial interests.

Correspondence and requests for materials should be addressed to J.F. (joerg.feikes@helmholtz-berlin.de) or C.T. (tang.xuh@tsinghua.edu.cn).

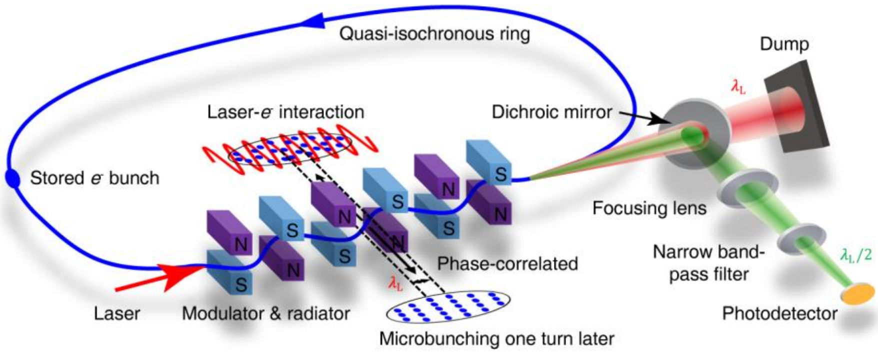

Fig 1 | Schematic of the experimental set-up. The stored 250 MeV electron bunches are energy-modulated by a 1064-nm-wavelength laser in an undulator, and become microbunched after one complete revolution in the 48-m-circumference quasi-isochronous storage ring. The undulator radiation from the electron bunches is separated into the fundamental and second harmonics by dichroic mirrors, and the signal detection focuses on the second harmonic. A 532-nm-center-wavelength 3-nm-FWHM-bandwidth narrow band-pass filter can be inserted in front of the photodetector to pick out the narrowband coherent radiation generated from the microbunching.

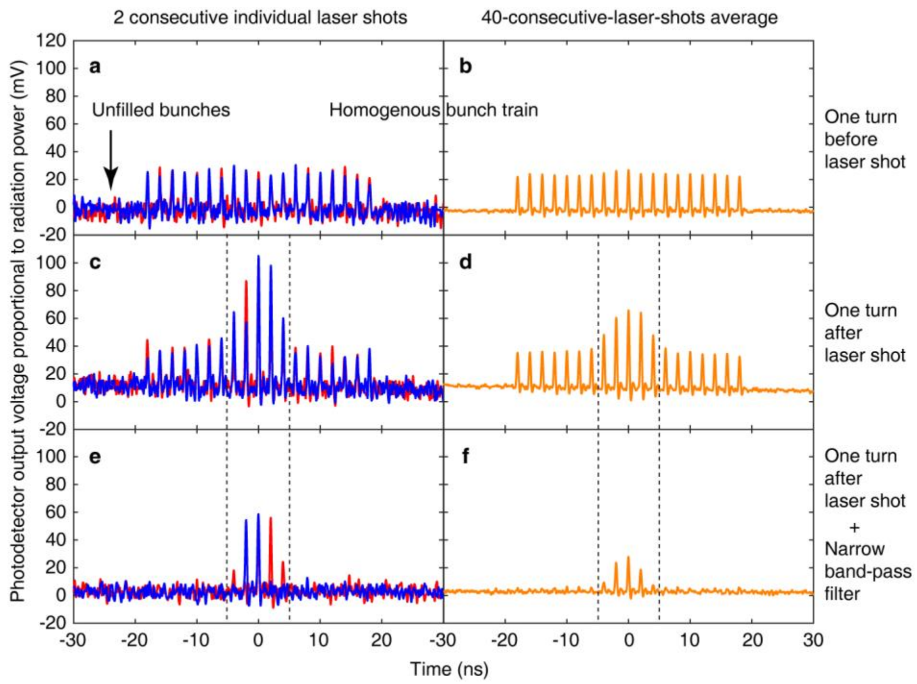

Fig 2 | Waveforms of the undulator radiation produced from a homogenous stored bunch train. a, b, The radiation one turn before the laser shot. **c**, **d,** The radiation one turn after the laser shot from the same bunches as that of **a** and **b**, in which the central five bunches are modulated by the laser pulse. The offset and general slight decreasing trend of the waveforms are because that the photodetector is saturated by the stray light of the modulation laser one revolution ago and is not completely recovered. **e**, **f,** The radiation one turn after the laser shot with a 532-nm-center-wavelength 3-nm-FWHM-bandwidth narrow band-pass filter placed in front of the photodetector, with the bunch filling and charge similar to that in **a** ~ **d**.

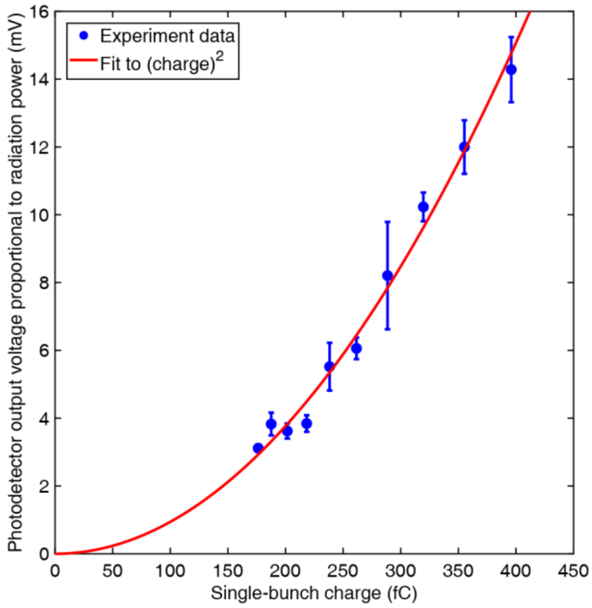

Fig. 3 | Quadratic bunch-charge dependence of the coherent undulator radiation generated from microbunching. The blue dots represent the experimental data and the red curve is a quadratic fit. Each data point represents the averaged result of 200 consecutive laser shots. The error bar denotes the standard deviation of the averaged results, when the averaging time window shifts for ±100 consecutive laser shots from the corresponding data point.

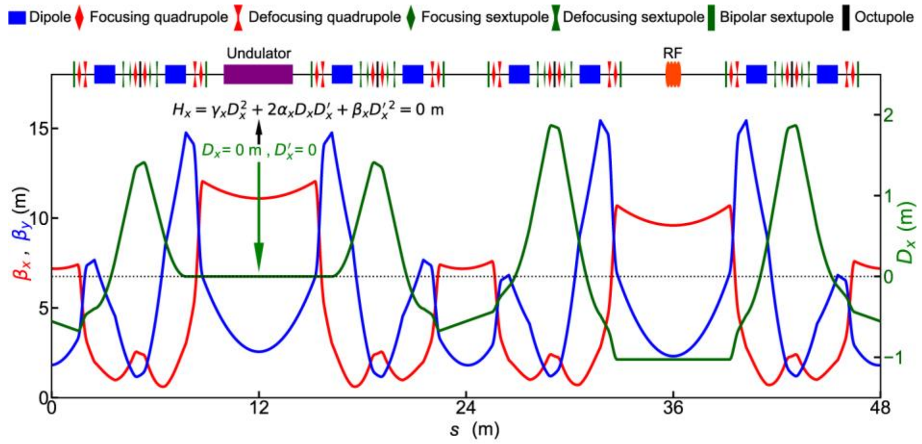

Extended Data Fig. 1 | The MLS quasi-isochronous magnet lattice used to generate microbunching. The magnet lattice and the legends are shown at the top. The curves are the model horizontal (red) and vertical (blue) β-functions as well as horizontal dispersion D_x (green). Operating parameters of the ring: beam energy $E_0 = 250$ MeV, relative energy spread $\sigma_\delta = 1.8 \times 10^{-4}$ (model), horizontal emittance $\varepsilon_x = 31$ nm (model), horizontal betatron tune $\nu_x = 3.18$ (model and measured), vertical betatron tune $\nu_y = 2.23$ (model and measured), horizontal chromaticity $\xi_x = -0.5$ (measured).

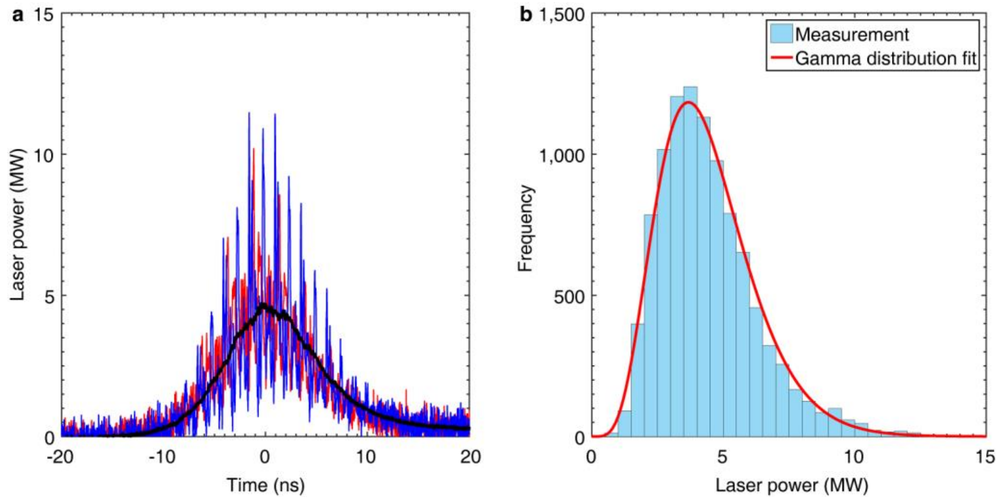

Extended Data Fig. 2 | Fluctuating temporal profiles of the multi-longitudinal-mode laser. a, The temporal profiles of two example consecutive laser shots (red and blue) and the averaged waveform of 200 consecutive laser shots (black). **b,** The statistical distribution of the laser power at $t = 0$ ns in **a** for 10000 consecutive laser shots, in which the red curve is a gamma distribution fit. Laser: compact Nd:YAG Q-switched laser (Beamtech Optronics Dawa-200). Detector: ultrafast photodetectors (Alphas UPS-40-UVIR-D, rise time < 40 ps). Measurement system: digital oscilloscope (Teledyne LeCroy WM825Zi-B, 25 GHz bandwidth, 80 GS/s sample rate).

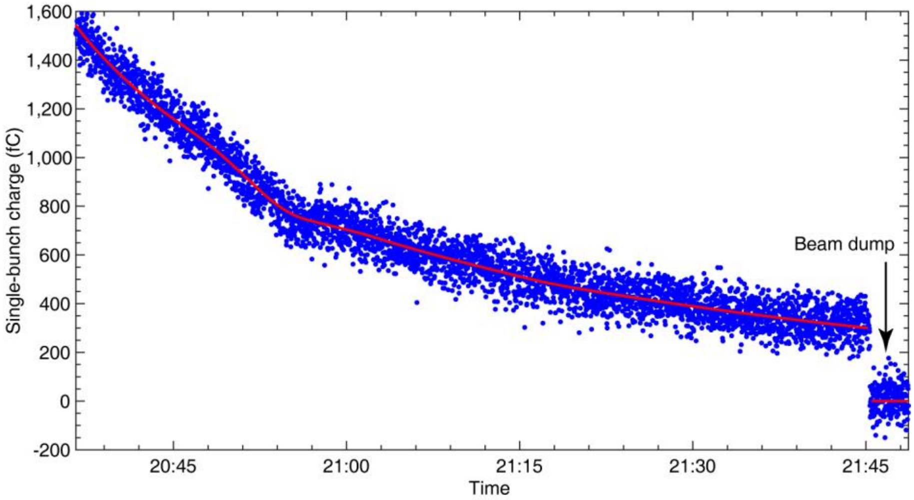

Extended Data Fig. 3 | Bunch charge measurement and evaluation. Blue dots are the measurement results with the systematic offset subtracted and the red curve is a fit by the sum of two exponential functions $Q(t) = Q_1 \exp(-t/\tau_1) + Q_2 \exp(-t/\tau_2)$ performed at different time intervals, with the fit results connected smoothly.

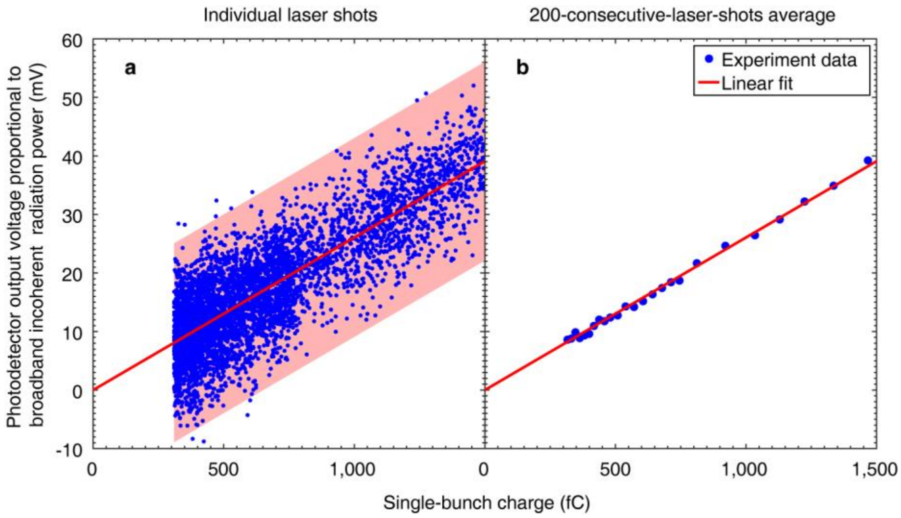

Extended Data Fig. 4 | Linear bunch-charge dependence of the broadband incoherent undulator radiation. a, The result corresponding to each individual laser shots and the shade (light red) represents 3σ of the detection noise. **b**, The result after taking a 200-consecutive-laser-shots averaging. The blue dots are the experimental data of a bunch not modulated by the laser and the red curves are linear fits.

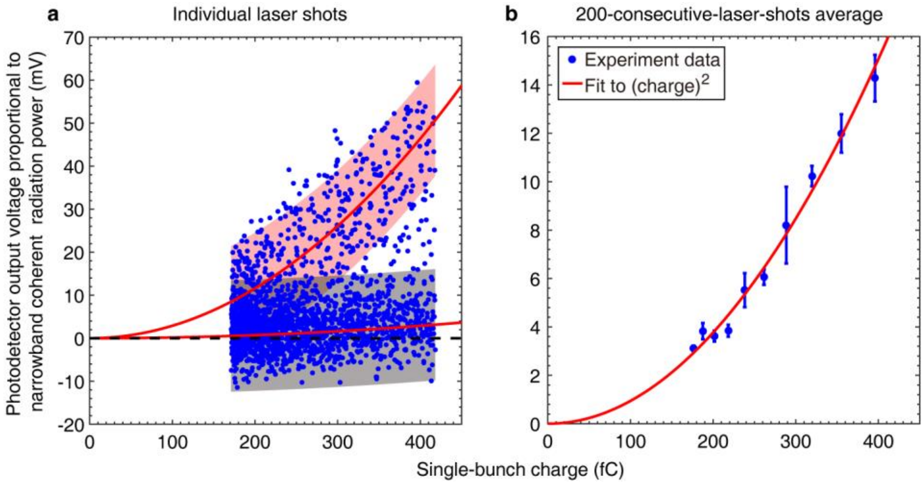

Extended Data Fig. 5 | Quadratic bunch-charge dependence of the narrowband coherent undulator radiation generated from microbunching. a, The result corresponding to each individual laser shots and the shades (light red and grey) represent the 3σ of the detection noise. **b,** The result after implementing a 200-consecutive-laser-shots averaging, which is the same as Fig. 3 and presented here again for convenient comparison with **a** and the incoherent signal in Extended Data Fig. 4. The blue dots represent the experimental data and the red curves are quadratic fits.